Quarkonium Production and Cold Matter Effects in pp, dA and AA Collisions

R. Vogt

Nuclear Science Division, Lawrence Berkeley National Laboratory, Berkeley, CA

Physics Department, University of California, Davis, CA

Outline

- Quarkonium Production in the Color Evaporation Model
- Baseline Nuclear Effects on Quarkonium Production
  - Initial-State Shadowing
  - Final-State Absorption
- Comparison to RHIC pp, d+Au and AA Data
- Predictions for J/ψ and Υ at the LHC

Production: Color Evaporation Model (CEM)

Gavai *et al.*, G. Schuler and R.V.

All quarkonium states are treated like $Q\overline{Q}$ below $H\overline{H}$ threshold

Distributions (x_F, p_T, $\sqrt{S}$, A) for all quarkonium family members identical — leads to constant ratios

At LO, $gg \to Q\overline{Q}$ and $q\overline{q} \to Q\overline{Q}$; NLO add $gq \to Q\overline{Q}q$

$$\sigma_C^{\rm CEM} = F_C \sum_{i,j} \int_{4m^2}^{4m_H^2} d\hat{s} \int dx_1 dx_2 \; f_{i/p}(x_1,\mu^2) \; f_{j/p}(x_2,\mu^2) \; \hat{\sigma}_{ij}(\hat{s}) \; \delta(\hat{s} - x_1 x_2 s)$$

F_C fixed at NLO from total cross section data as a function of $\sqrt{S}$, $\sigma(x_F > 0)$ for inclusive J/ψ and $B_{\mu\mu} d\sigma(\Upsilon + \Upsilon' + \Upsilon'')_{y=0}/dy$

Values of m and μ (here $\mu \propto \sqrt{(p_{T\,Q}^2 + p_{T\,\overline{Q}}^2)/2 + m_Q^2} = m_{T\,Q\overline{Q}} \equiv m_T$ in the exclusive $Q\overline{Q}$ code) for several parton densities fixed from $Q\overline{Q}$ production

$\chi_c/J/\psi$ Ratio Energy Independent

HERA-B comparison of $R_{\chi_c} = \sigma(\chi_c)/\sigma(J/\psi)$ with πA and pA data

Result consistent with R_{χ_c} independent of $\sqrt{S}$, predicted by CEM

CDF result, $R_{\chi_c} = 0.297 \pm 0.017 \pm 0.057$, consistent with fixed-target

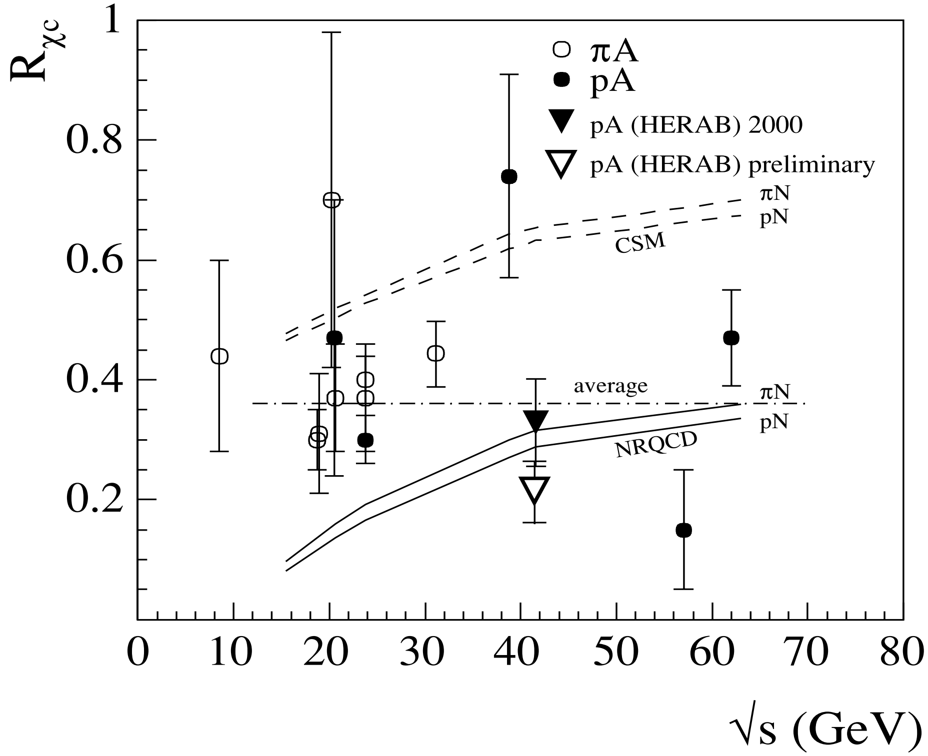

Figure 1: Ratio of χ_c to J/ψ cross sections as a function of $\sqrt{S}$ for πA and pA fixed-target measurements. The CSM and NRQCD curves are obtained from Monte Carlo while the 'average' is the average value of all measurements. From I. Abt *et al.* (HERA-B Collab.), Phys. Lett. **561** (2003) 61.

$\psi'/J/\psi$ Ratio Also Energy Independent

Data from pp and pA interactions
Horizontal line corresponds to CEM

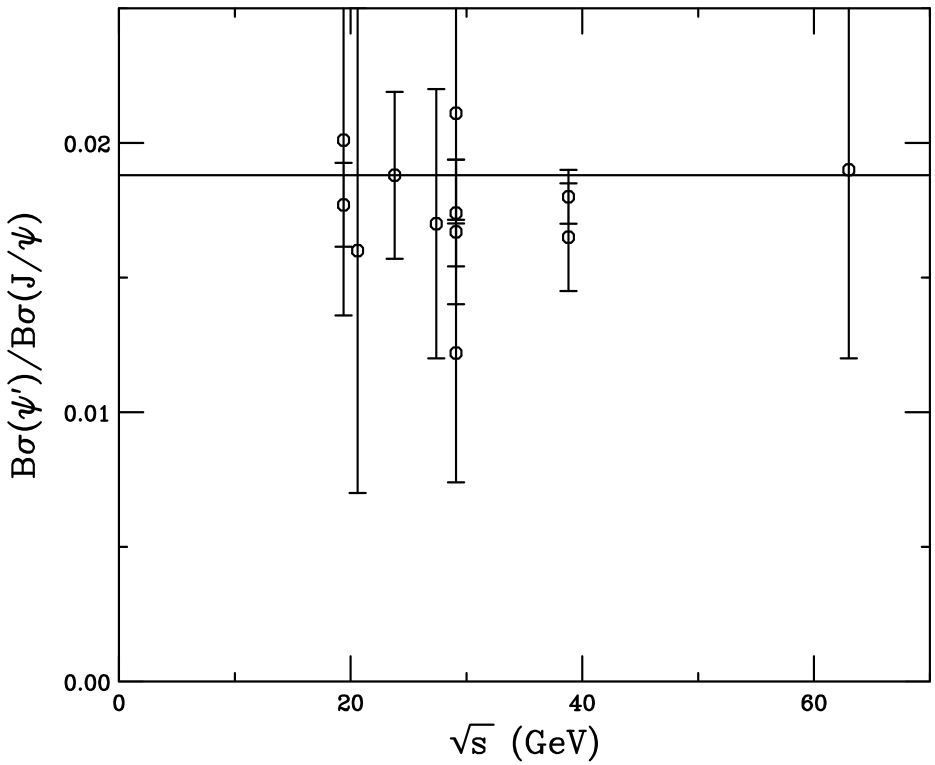

Figure 2: Ratio of ψ' to J/ψ cross sections to lepton pairs as a function of $\sqrt{S}$ for pp and pA measurements. Adapted from R.V., Phys. Rept. **310** (1999) 197.

Production and Feeddown Fractions

Data and branching ratios can be used to separate out the F_C's for each state in a quarkonium family

Resonance	$\sigma_i^{\rm dir}/\sigma_H$	f_i
J/ψ	**0.62**	**0.62**
ψ'	**0.14**	**0.08**
χ_{c1}	**0.6**	**0.16**
χ_{c2}	**0.99**	**0.14**
Υ	**0.52**	**0.52**
Υ'	**0.33**	**0.10**
Υ''	**0.20**	**0.02**
$\chi_b(1P)$	**1.08**	**0.26**
$\chi_b(2P)$	**0.84**	**0.10**

Table 1: The ratios of the direct quarkonium production cross sections, $\sigma_i^{\rm dir}$, to the inclusive J/ψ and Υ cross sections, denoted σ_H, and the feed down contributions of all states to the J/ψ and Υ cross sections, f_i. From Digal *et al.*, Phys. Rev. D **64** (2001) 094015.

Charmonium Parameters From $c\overline{c}$ Cross Sections

Use charm quark mass and renormalization/factorization scales that agree with $\sigma^{\rm tot}_{c\overline{c}}(\sqrt{S})$ as inputs to CEM

Proceedure favors lower charm quark mass

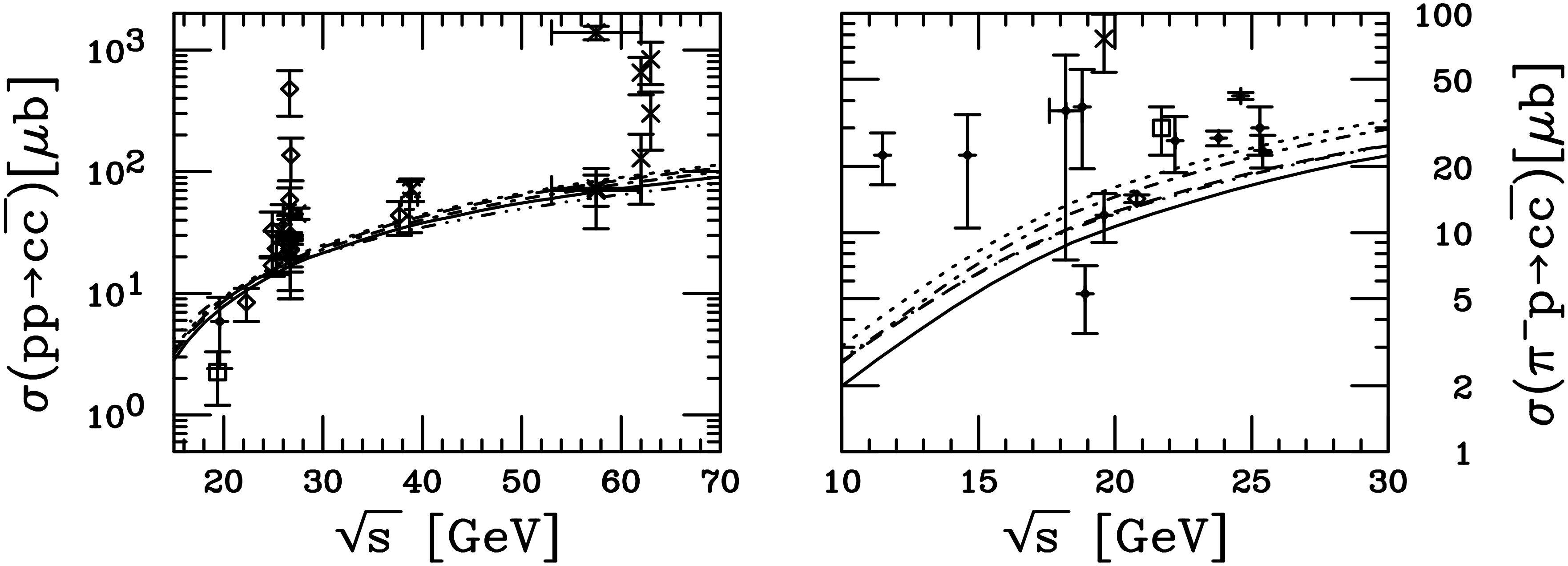

Figure 3: Total $c\overline{c}$ cross sections in pp and $\pi^- p$ interactions. The curves are: MRST HO with $\mu = m = 1.4$ GeV (solid) and $\mu = 2m = 2.4$ GeV (dashed); CTEQ 5M with $\mu = m = 1.4$ GeV (dot-dashed) and $\mu = 2m = 2.4$ GeV (dotted); and GRV 98 HO with $\mu = m = 1.3$ GeV.

Inclusive J/ψ F_C in the CEM

Case	PDF	m (GeV)	μ/m_T	$\sigma_{J/\psi}/\sigma_C^{\rm CEM}$
ψ1	MRST HO	1.2	2	0.0144
ψ2	MRST HO	1.4	1	0.0248
ψ3	CTEQ 5M	1.2	2	0.0155
ψ4	GRV 98 HO	1.3	1	0.0229

Table 2: The production fractions obtained from simultaneously fitting F_C to the J/ψ total cross sections and $y = 0$ cross sections as a function of energy. The PDF, charm quark mass, and scales used are obtained from comparison of the $c\overline{c}$ cross section to data.

Inclusive J/ψ Total Forward Cross Sections

Total forward J/ψ cross sections as a function of energy

Agrees well with PHENIX pp data at 200 GeV, a bit low for Run II CDF inclusive cross section

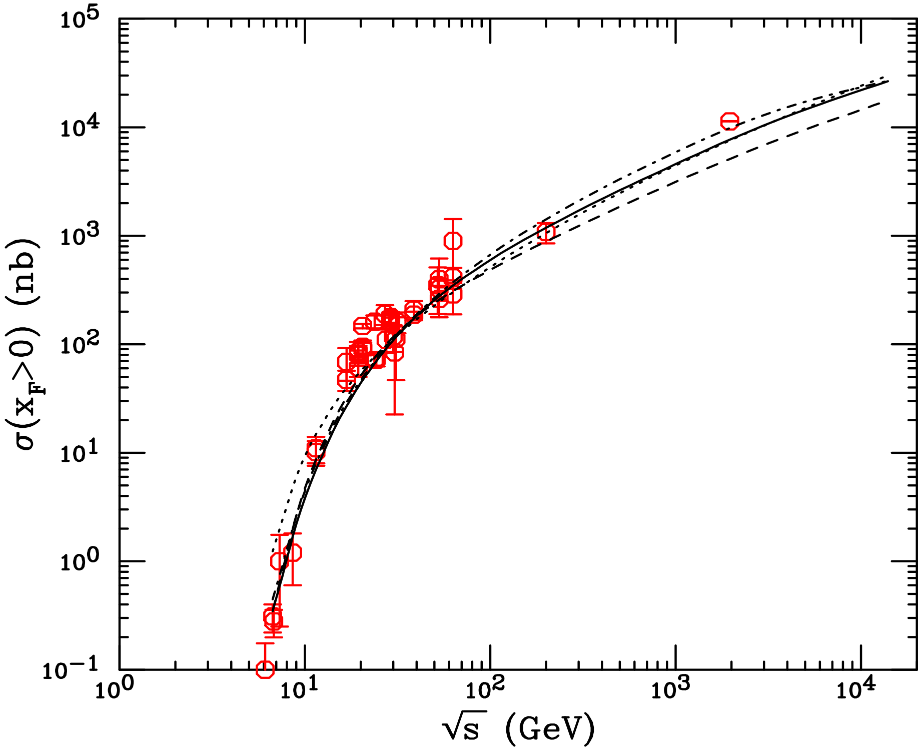

Figure 4: NLO J/ψ forward cross sections. The solid curve employs the MRST HO distributions with $m = 1.2$ GeV $\mu/m_T = 2$, the dashed, MRST HO with $m = 1.4$ GeV $\mu/m_T = 1$, the dot-dashed, CTEQ 5M with $m = 1.2$ GeV $\mu/m_T = 2$, and the dotted, GRV 98 HO with $m = 1.3$ GeV $\mu/m_T = 1$.

The Quarkonium p_T Distribution in the $Q\overline{Q}$ NLO Code

Gaussian k_T smearing, $\langle k_T^2 \rangle_p = 1$ GeV^2 for fixed target pp and πp, broadened for pA and AA, NLO code adds in final state:

$$g_p(k_T) = \frac{1}{\pi \langle k_T^2 \rangle_p} \exp(-k_T^2/\langle k_T^2 \rangle_p)$$

Comparison with J/ψ and Υ Tevatron Run I data at 1.8 TeV shows that the broadening should increase with energy, to $\langle k_T^2 \rangle_p \approx 2.5$ GeV^2

We make a simple linear extrapolation in $\sqrt{S}$ from $\sqrt{S_0} = 20$ GeV to obtain

$$\langle k_T^2 \rangle_p = 1 + \frac{1}{6} \ln \left(\frac{S}{S_0} \right) \mathrm{GeV}^2$$

Tevatron Run I Charmonium p_T Distributions

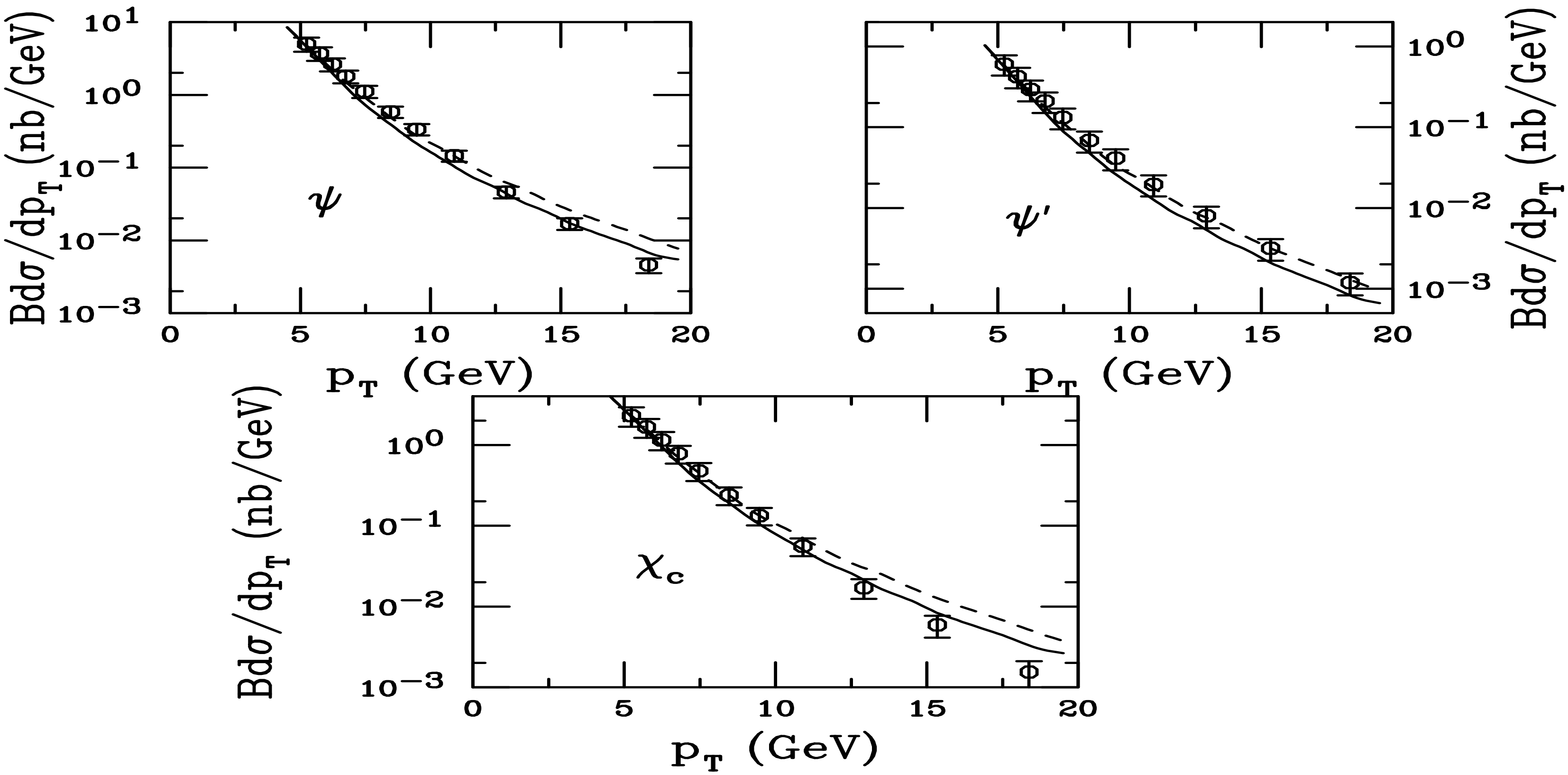

Figure 5: The p_T distributions of direct J/ψ as well as J/ψ's from ψ' and χ_c decays calculated for cases $\psi1$ (solid) and $\psi4$ (dashed) are compared to the CDF data (F. Abe *et al.*, Phys. Rev. Lett. **79** (1997) 578). We use $\langle k_T^2 \rangle_p = 2.5$ GeV^2.

Tevatron Run II Charmonium p_T Distributions

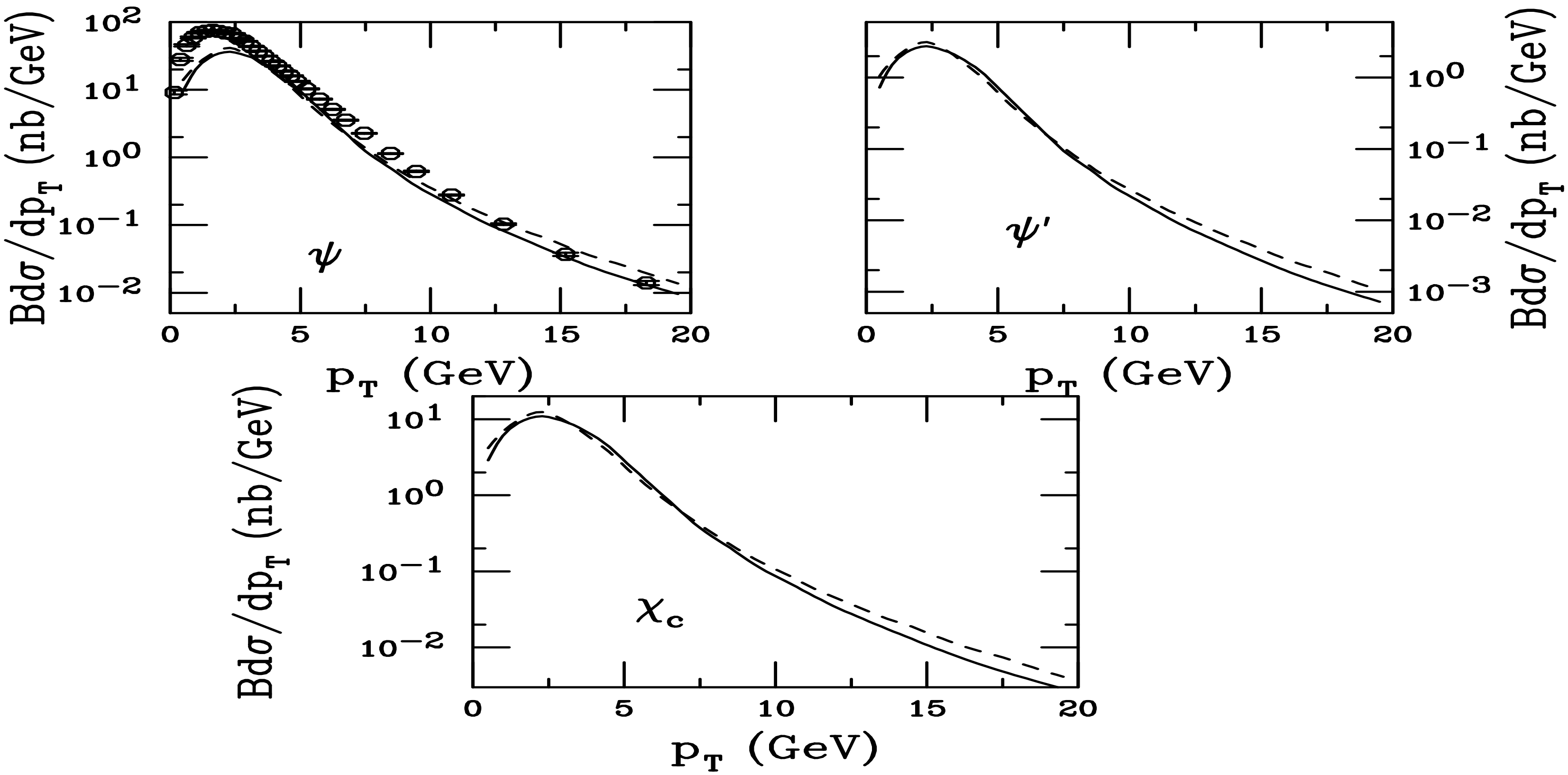

Figure 6: The inclusive J/ψ p_T distributions as well as J/ψ's from ψ' and χ_c decays calculated for cases $\psi1$ (solid) and $\psi4$ (dashed) are compared to the CDF data (D. Acosta *et al.*, Phys. Rev. D **71** (2005) 032001). We use $\langle k_T^2 \rangle_p = 2.5$ GeV^2.

Bottomonium Parameters from $b\bar{b}$ Cross Sections

Fewer $b\bar{b}$ total cross section data
Take $\mu = m = 4.75$ GeV and vary around central value for similar $\sigma_{b\bar{b}}^{\rm tot}(\sqrt{S})$

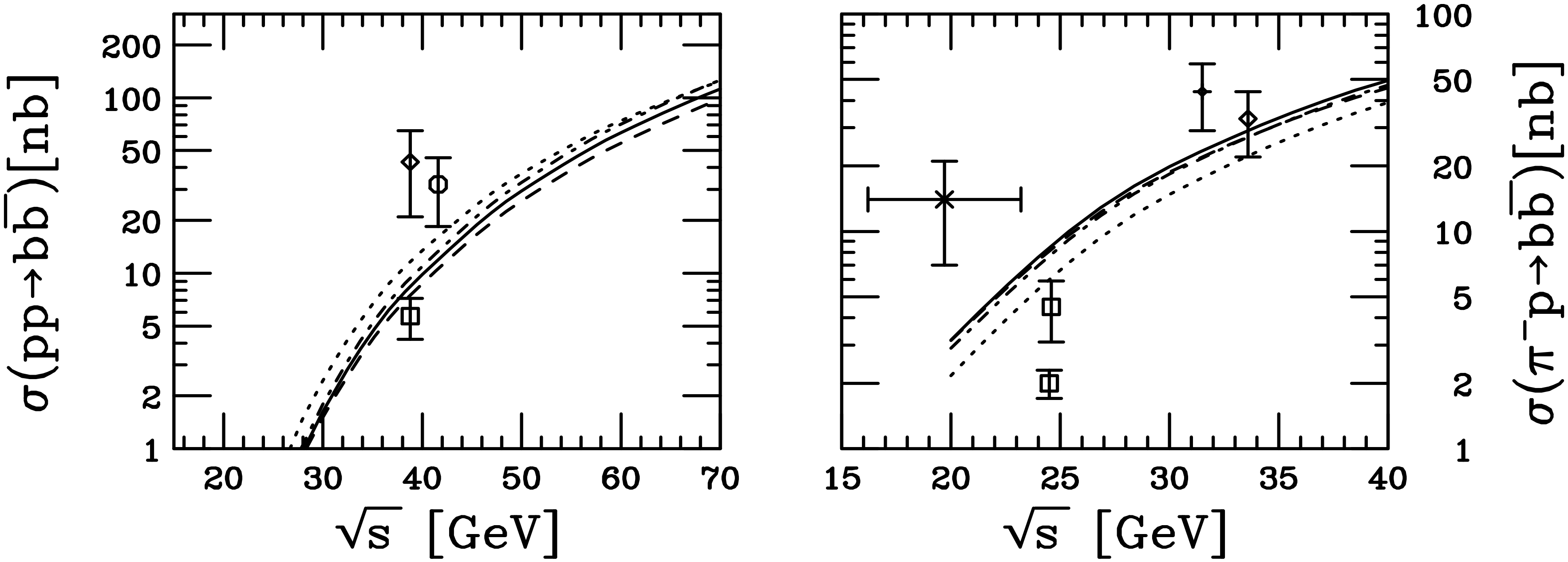

Figure 7: Total $b\bar{b}$ cross sections in pp and $\pi^- p$ interactions. The curves are: MRST HO with $\mu = m = 4.75$ GeV (solid), $\mu = 2m = 9$ GeV (dashed), and $\mu = m/2 = 2.5$ GeV (dot-dashed); GRV 98 HO with $\mu = m = 4.75$ GeV.

Inclusive Υ F_C in the CEM

Case	PDF	m (GeV)	μ/m_T	$\sigma_{B\sum\Upsilon}/\sigma_b^{\rm CEM}$	$\sigma_\Upsilon/\sigma_b^{\rm CEM}$
Υ1	MRST HO	4.75	1	0.000963	0.0276
Υ2	MRST HO	4.50	2	0.000701	0.0201
Υ3	MRST HO	5.00	0.5	0.001766	0.0508
Υ4	GRV 98 HO	4.75	1	0.000787	0.0225

Table 3: The production fractions obtained from fitting the CEM cross section to the combined Υ cross sections to muon pairs at $y = 0$ as a function of energy. The PDF, charm quark mass, and scales used are the same as those obtained by comparison of the $b\overline{b}$ cross section to data.

Inclusive Υ Cross Sections at $y = 0$

Cross sections include all $\Upsilon(nS)$ states and their decays to muon pairs

Data is from pp interactions except for highest two points where only $p\overline{p}$ colliders available

At high energies, $gg \to Q\overline{Q}$ dominates and differences between $p\overline{p} \to \Upsilon$ and $pp \to \Upsilon$ are negligible

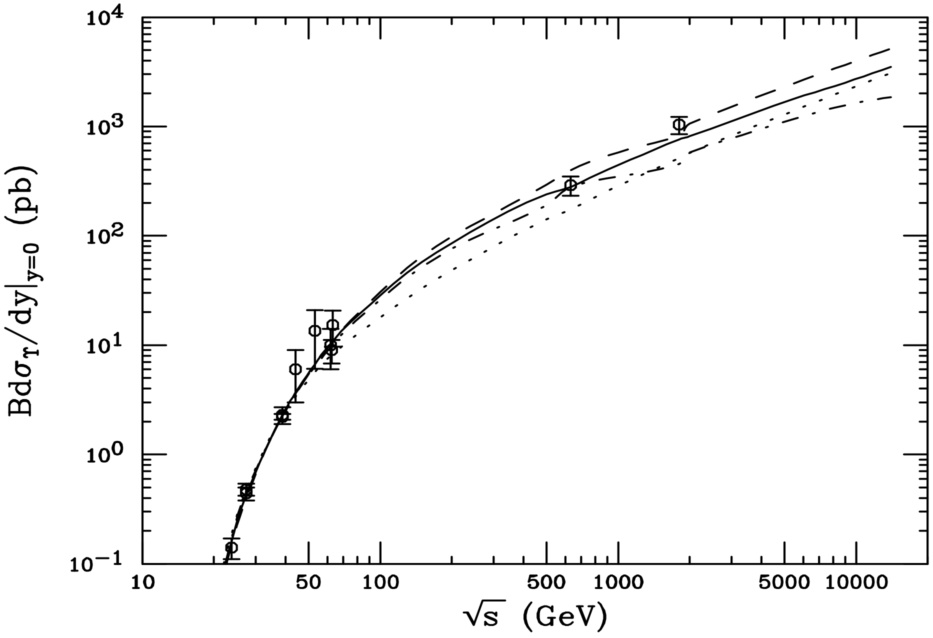

Figure 8: Inclusive Υ production data, combined from all three S states, and compared to NLO CEM calculations. The solid curve employs the MRST HO distributions with $m = 4.75$ GeV $\mu/m_T = 1$, the dashed, $m = 4.5$ GeV $\mu/m_T = 0.5$, the dot-dashed, $m = 5$ GeV $\mu/m_T = 2$, and the dotted, GRV 98 HO with $m = 4.75$ GeV $\mu/m_T = 1$.

Tevatron Run I Υ p_T Distributions

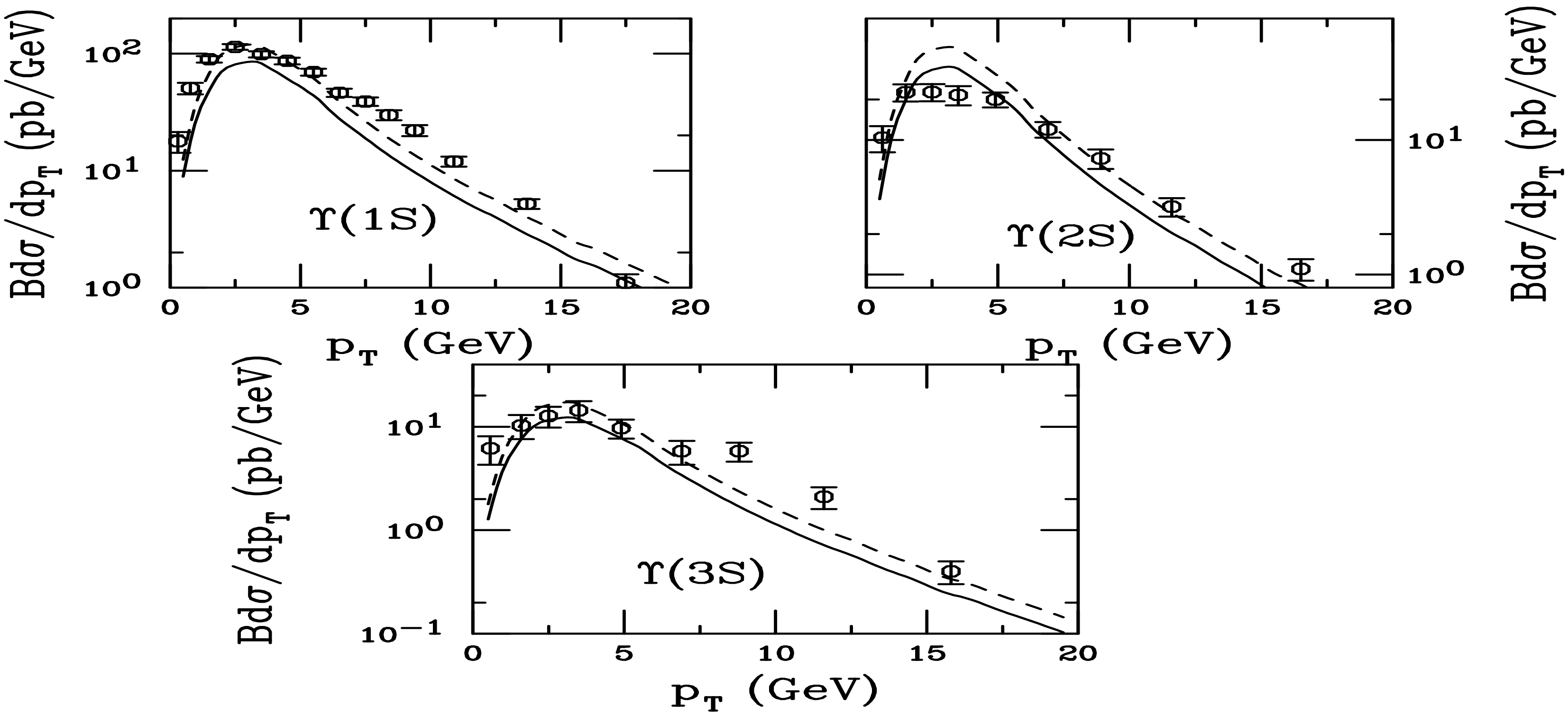

Figure 9: The p_T distributions of inclusive $\Upsilon(1S)$, $\Upsilon(2S)$ and $\Upsilon(3S)$ calculated for case $\Upsilon1$ with $\langle k_T^2 \rangle_p = 3$ GeV^2 are compared to the CDF data (D. Acosta *et al.* Phys. Rev. Lett. **88** (2002) 161802). The dashed curve is multiplied by a K factor of 1.4.

Prediction of J/ψ Rapidity Distributions at RHIC

Agreement of CEM with overall normalization of Run 3 data good
Shape has right trend for d+Au with EKS98 shadowing

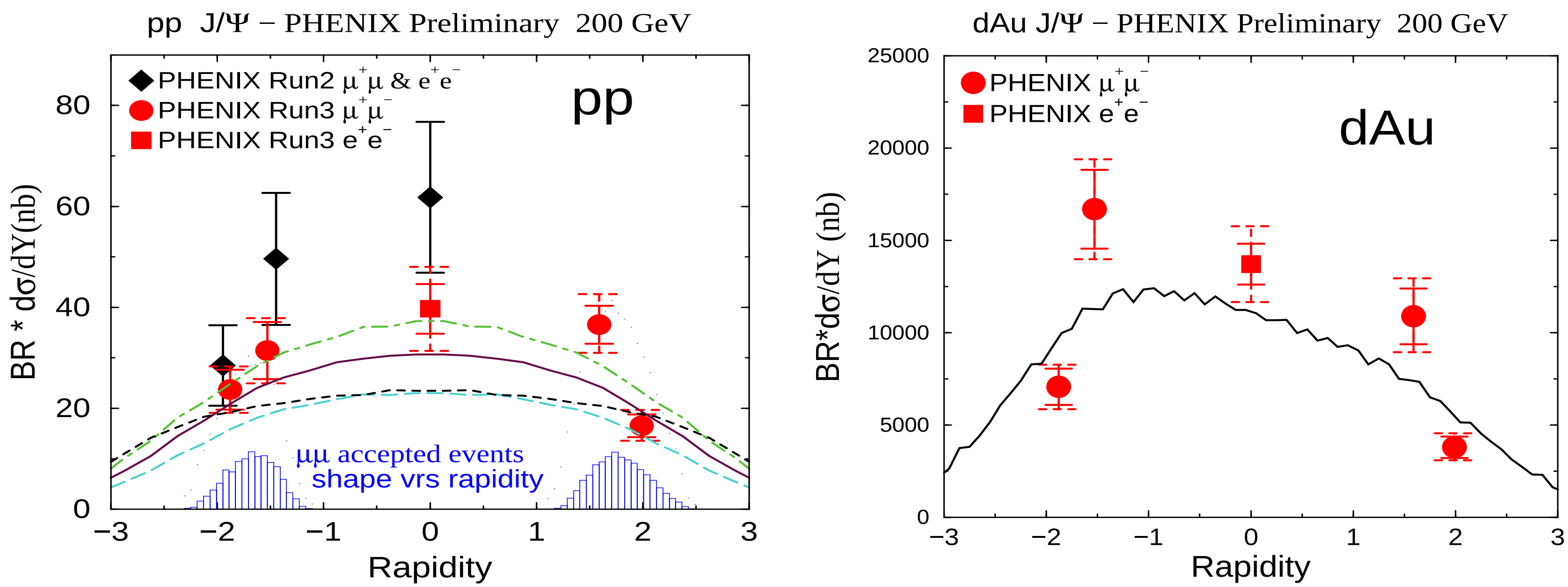

Figure 10: The inclusive J/ψ y distributions in $\sqrt{S} = 200$ pp (left-hand side for $\psi 1$ (solid), $\psi 2$ (dashed), $\psi 3$ (dot-dashed) and $\psi 4$ (dotted)) and d+Au (right-hand side with $\psi 1$ and EKS98) interactions. Plots courtesy of Mike Leitch.

Nuclear Effects Important in dA and AA Interactions

Nuclear effects on charmonium important in fixed-target interactions

Parameterizing $\sigma_{pA} = \sigma_{pp} A^\alpha$, $\alpha(x_F, p_T)$

For $\sqrt{S_{NN}} \leq 40$ GeV and $x_F > 0.25$, α decreases strongly with x_F

Consider two low x_F cold matter effects at colliders:

- **Nuclear Shadowing — initial-state effect on the parton distributions affecting total rate, important as a function of y/x_F**
- **Absorption — final-state effect, after $c\overline{c}$ that forms the J/ψ has been produced, pair breaks up in matter due to interactions with nucleons**

Including shadowing for $\sqrt{S} \geq 38$ GeV makes $\alpha < 1$ for $x_F/y > 0$, hence reducing the absorption cross section needed

At high x_F, other mechanisms (energy loss, intrinsic charm) may be important but $x_F > 0.25$ corresponds to $y > 2.8$ at 200 GeV (larger y for higher $\sqrt{S}$) and do not appear in p_T-integrated y distributions

Nuclear Parton Distributions

Nuclear parton densities

$$
\begin{aligned}
F_i^A(x,Q^2,\vec{r},z) &= \rho_A(s) S^i(A,x,Q^2,\vec{r},z) f_i^N(x,Q^2) \\
s &= \sqrt{r^2+z^2} \\
\rho_A(s) &= \rho_0 \frac{1+\omega(s/R_A)^2}{1+\exp[(s-R_A)/d]}
\end{aligned}
$$

We use EKS98, Frankfurt, Guzey and Strikman (FGSo, FGSh, and FGSl) and DeFlorian and Sassot (nDS and nDSg)

EKS98, FGSo, nDS and nDSg have no spatial dependence, FGSh and FGSl do

With no nuclear modifications, $S^i(A,x,Q^2,\vec{r},z) \equiv 1$

Assume spatial dependence proportional to nuclear path length:

$$
S^i_\rho(A,x,Q^2,\vec{r},z) = 1 + N_\rho (S^i(A,x,Q^2) - 1) \frac{\int dz \rho_A(\vec{r},z)}{\int dz \rho_A(0,z)}
$$

Normalization: $(1/A)\int d^2r dz \rho_A(s) S^i_\rho \equiv S^i$**. Larger than average modifications for** $s=0$**. Nucleons like free protons when** $s \gg R_A$**. Similar normalization for spatial dependence of FGS.**

Comparing Shadowing Parameterizations: x Dependence

EKS98, nDS and nDSg for all A, FGS for $A = 12, 40, 110$ and 197/206

Ratios shown for GRV98 scales, $\mu = 1.3$ and 4.75 GeV for charm and bottom but if $\mu < \mu_0$ for set, take $\mu = \mu_0$

EKS98 and nDSg similar for $A = 208$ but nDSg weaker for smaller A

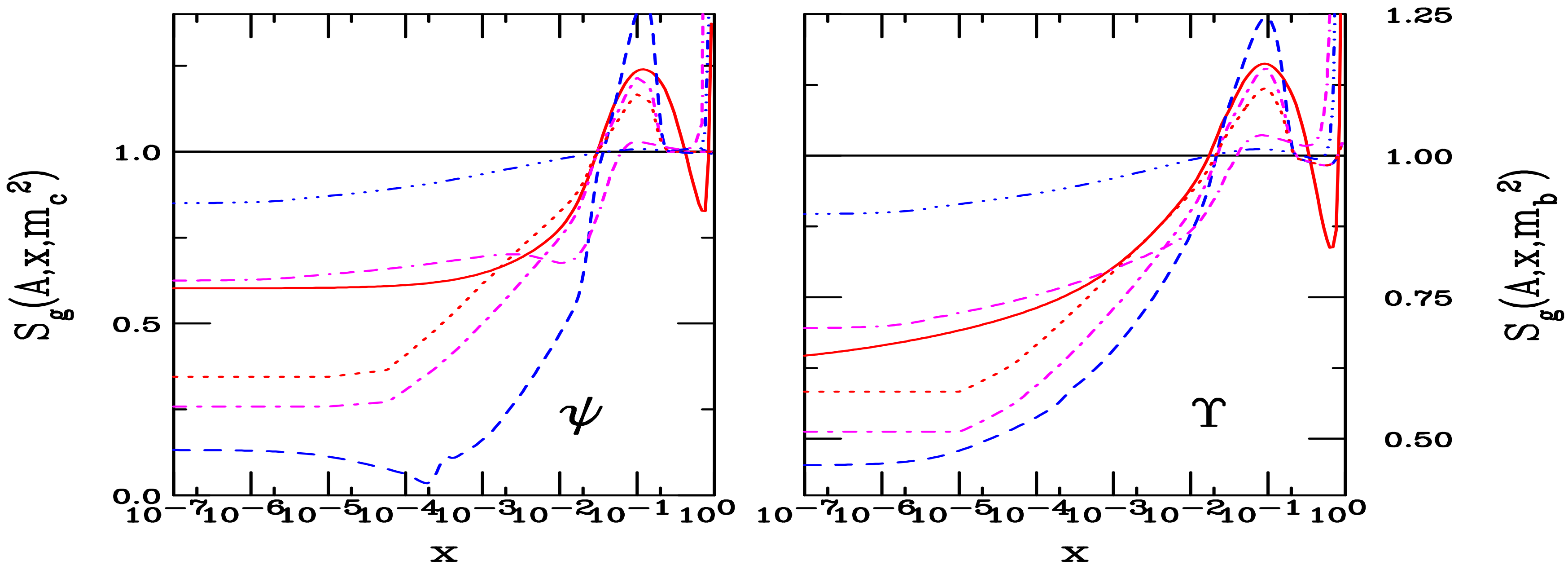

Figure 11: Shadowing parameterizations for J/ψ (left) and Υ (right) scales for $A = 208$. The parameterizations are EKS98 (solid red), FGSo (dashed blue), FGSh (dot-dashed magenta), FGSl (dotted red), nDS (dot-dot-dot-dashed blue) and nDSg (dash-dash-dash dotted magenta).

Average x_2 as a Function of Energy and Rapidity

We calculate $\langle x_2 \rangle$ as a function of rapidity in the CEM (N.B. $\langle x_1 \rangle$ is mirror imagine of $\langle x_2 \rangle$)

Increasing $\sqrt{S}$ broadens y range and decreases x_2

For J/ψ at forward rapidity, lower $\langle x_2 \rangle$ reached than with leading hadrons since gg dominates and scale is relatively lower

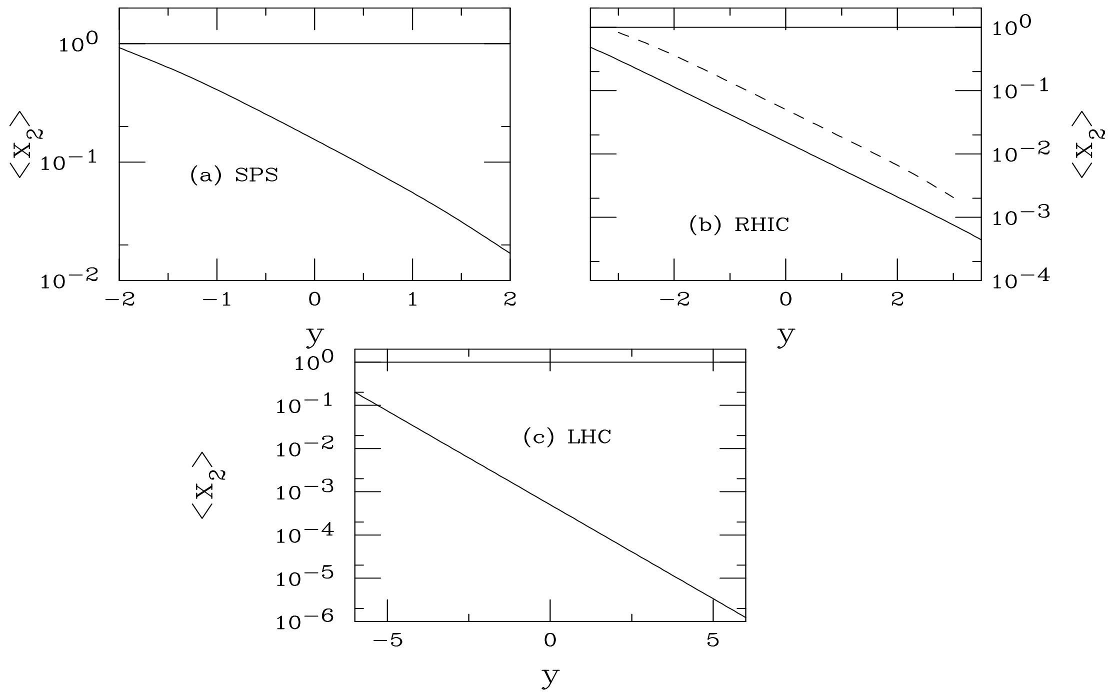

Figure 12: We give the average value of the nucleon momentum fraction, x_2, in *pp* collisions as a function of rapidity for (a) the CERN SPS with $\sqrt{S} = 19.4$ GeV, (b) RHIC with $\sqrt{S} = 200$ GeV and (c) the LHC with $\sqrt{S} = 6.2$ TeV.

Quarkonium Absorption by Nucleons

Woods-Saxon nuclear density profiles typically used

$$\begin{aligned}\sigma_{pA} &= \sigma_{pN} \int d^2b \int_{-\infty}^{\infty} dz\, \rho_A(b,z) S_A^{\rm abs}(b) \\ &= \sigma_{pN} \int d^2b \int_{-\infty}^{\infty} dz\, \rho_A(b,z) \exp\left\{- \int_z^{\infty} dz' \rho_A(b,z') \sigma_{\rm abs}(z'-z)\right\}\end{aligned}$$

Note that if $\rho_A = \rho_0$, $\alpha = 1 - 9\sigma_{\rm abs}/(16\pi r_0^2)$

The value of $\sigma_{\rm abs}$ depends on the parameterization of σ_{pA} – Glauber, hard sphere, A^α etc. (shown by NA50)

Initial-state shadowing not taken into account at SPS energies, increasing $\sqrt{S_{NN}}$ and rapidity range of measurement influences total shadowing effect: could make effective $\sigma_{\rm abs}$ without shadowing depend on y, $\sqrt{S_{NN}}$

Absorption Models Influenced by Production Mechanism

singlet: Individual charmonium cross sections grow quadratically with proper time until formation time; only effective when state can form in target – no effect when formed outside

octet: $|(c\overline{c})_8 g\rangle$ "pre-resonance" travels through nucleus, $(c\overline{c})_8$ can dissociate before final state forms; assume either "constant" (y independent) or "growing", (octet to singlet conversion inside target for $y < 0$) – little difference at collider energy; A dependence same for all final states

NRQCD: Nonrelativistic QCD approach differs from CEM in that states are produced with fixed singlet and octet contributions (J/ψ and ψ' predominantly octet, χ_c singlet so J/ψ and χ_c A dependence should be different)

Simultaneous measurement of J/ψ and χ_c A dependence would help determine the production mechanism (CEM vs. NRQCD)

Rapidity Dependence of Absorption Alone

Results shown for inclusive and direct J/ψ, ψ' and χ_c

Constant and growing octet indistinguishable in detector range, singlet absorption only effective for $y < -1$, NRQCD also shows little rapidity dependence

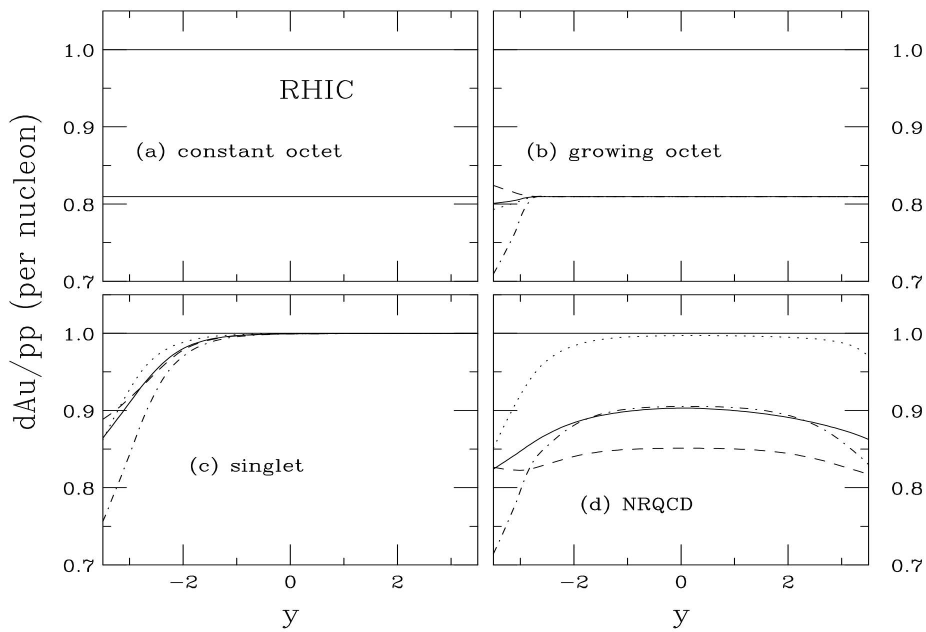

Figure 13: The J/ψ dAu/pp ratio at 200 GeV as a function of rapidity for absorption alone. We show (a) constant octet with 3 mb, (b) growing octet with 3 mb asymptotic cross section for all states, (c) singlet with 2.5 mb J/ψ absorption cross section, all calculated in the CEM and (d) NRQCD with a combination of octet and singlet matrix elements. The curves show total J/ψ (solid), direct J/ψ (dashed), ψ' (dot-dashed) and χ_c (dotted).

Setting Baseline Cold Nuclear Matter Effects at RHIC: In Collaboration with Mike Leitch

Determine balance of shadowing and absorption from RHIC data

Compare combinations of shadowing parameterizations and absorption cross sections to RHIC d+Au data

Make χ^2 fits to $R_{\rm dAu}(y)$, $R_{\rm dAu}(N_{\rm coll})$ for all combinations – are some parameterizations more favored than others?

Take results with relative best agreement to determine the maximum range of cold nuclear matter effects in AA collisions

This becomes baseline onto which hot matter effects of color screening and recombination can be added

Results shown here for EKS98 and nDSg shadowing since their shapes are most compatible with the data

Absorption and Shadowing at RHIC: $R_{\rm dAu}(y)$

EKS98 and nDSg compared to d+Au data with $0 < \sigma_{\rm abs} < 3$ mb and MRST parton densities with $m = 1.2$ GeV, $\mu = 2m_T$

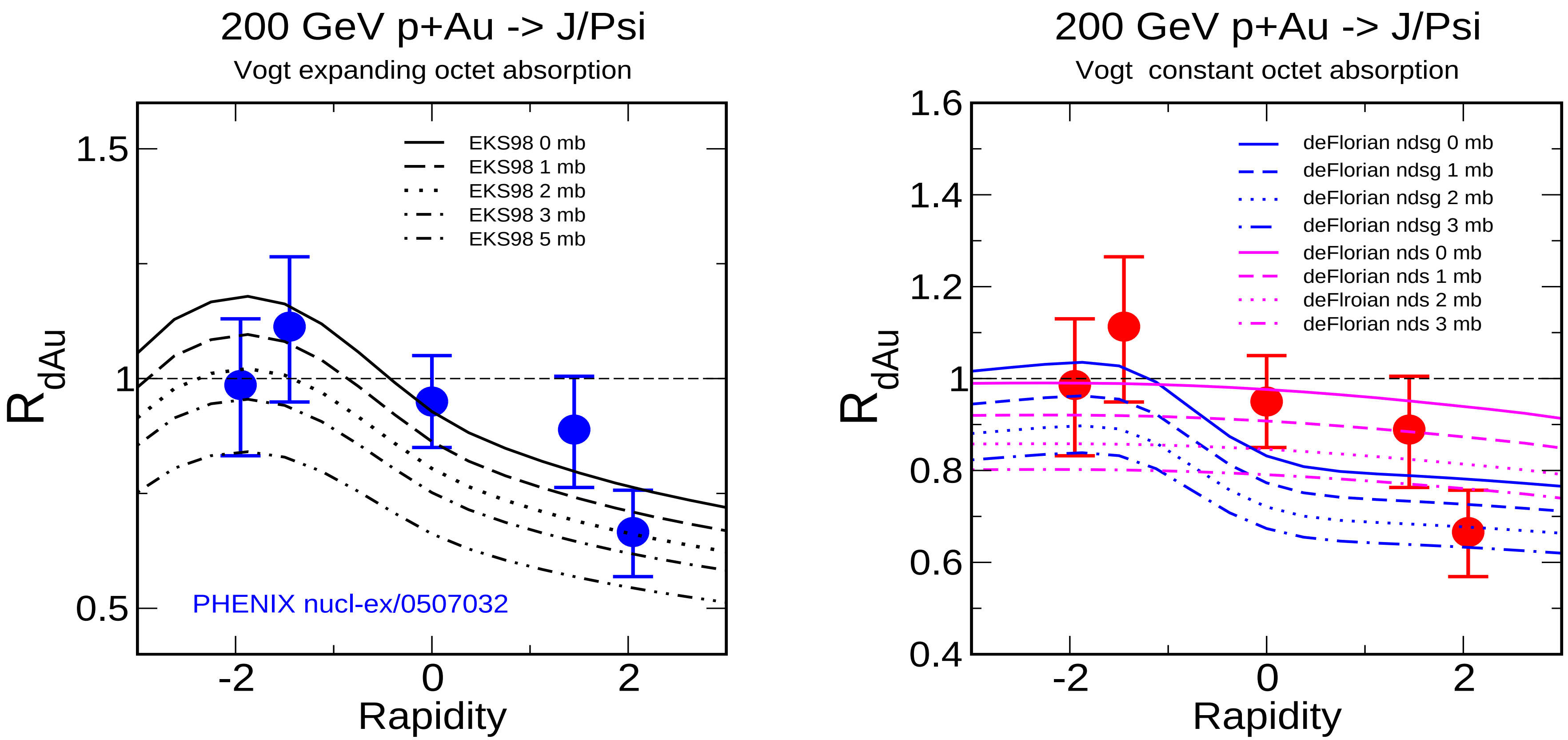

Figure 14: Octet absorption for $0 \leq \sigma_{\rm abs} \leq 3$ mb calculated with EKS98 (left) and nDSg (right) using the MRST PDFs and $m = 1.2$ GeV, $\mu = 2m_T$ compared to PHENIX data. (An additional overall normalization error of 12% is not shown.) RV and Mike Leitch, in progress.

Absorption and Shadowing at RHIC: $R_{\rm AA}(y)$

Larger difference between EKS98 and nDSg for Au+Au than Cu+Cu

General trends of cold matter effects similar to data

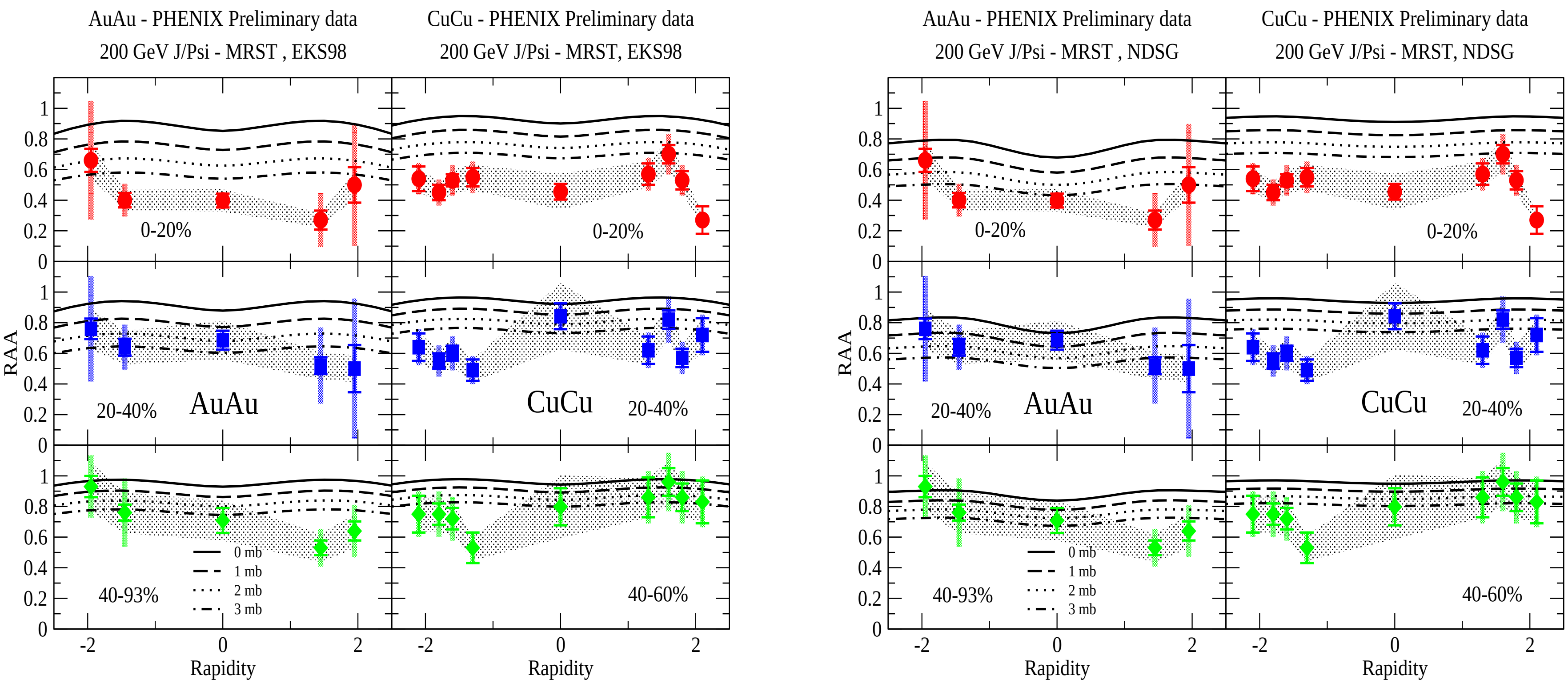

Figure 15: Octet absorption for $0 \leq \sigma_{\rm abs} \leq 3$ mb (top to bottom) calculated with EKS98 (left) and nDSg (right) with the MRST PDFs and $m = 1.2$ GeV, $\mu = 2m_T$. PHENIX data (QM'05) are shown for Au+Au and Cu+Cu collisions at 200 GeV. The absolute normalization uncertainty is shown by the grey bands. RV and Mike Leitch, in progress.

Centrality Dependence of Shadowing and Absorption

PHENIX d+Au results presented as a function of the number of binary nucleon-nucleon collisions, $N_{\rm coll}$, the convolution of the nuclear profile functions multiplied by the inelastic NN cross section, 42 mb at RHIC

$$N_{\rm coll}(b) = \sigma_{NN}^{\rm in} \int d^2s T_A(s) T_B(|\vec{b} - \vec{s}|)$$

AA results presented as a function of the number of nucleon participants, $N_{\rm part}$,

$$N_{\rm part}(b) = \int d^2s [T_A(s)(1 - \exp(-\sigma_{NN} T_B(|\vec{b} - \vec{s}|))) + T_B(|\vec{b} - \vec{s}|)(1 - \exp(-\sigma_{NN} T_A(s)))]$$

Results with EKS98 and nDSg compared at $y = -1.7$ (antishadowing), 0 (transition region) 1.7 (shadowing)

Absorption and Shadowing at RHIC: $R_{\mathrm{dAu}}(N_{\mathrm{coll}})$

Centrality dependence of shadowing alone generally stronger for nDSg at $y = -1.7$, 0, similar for $y = 1.7$

Data do not help distinguish between different σ_{abs}

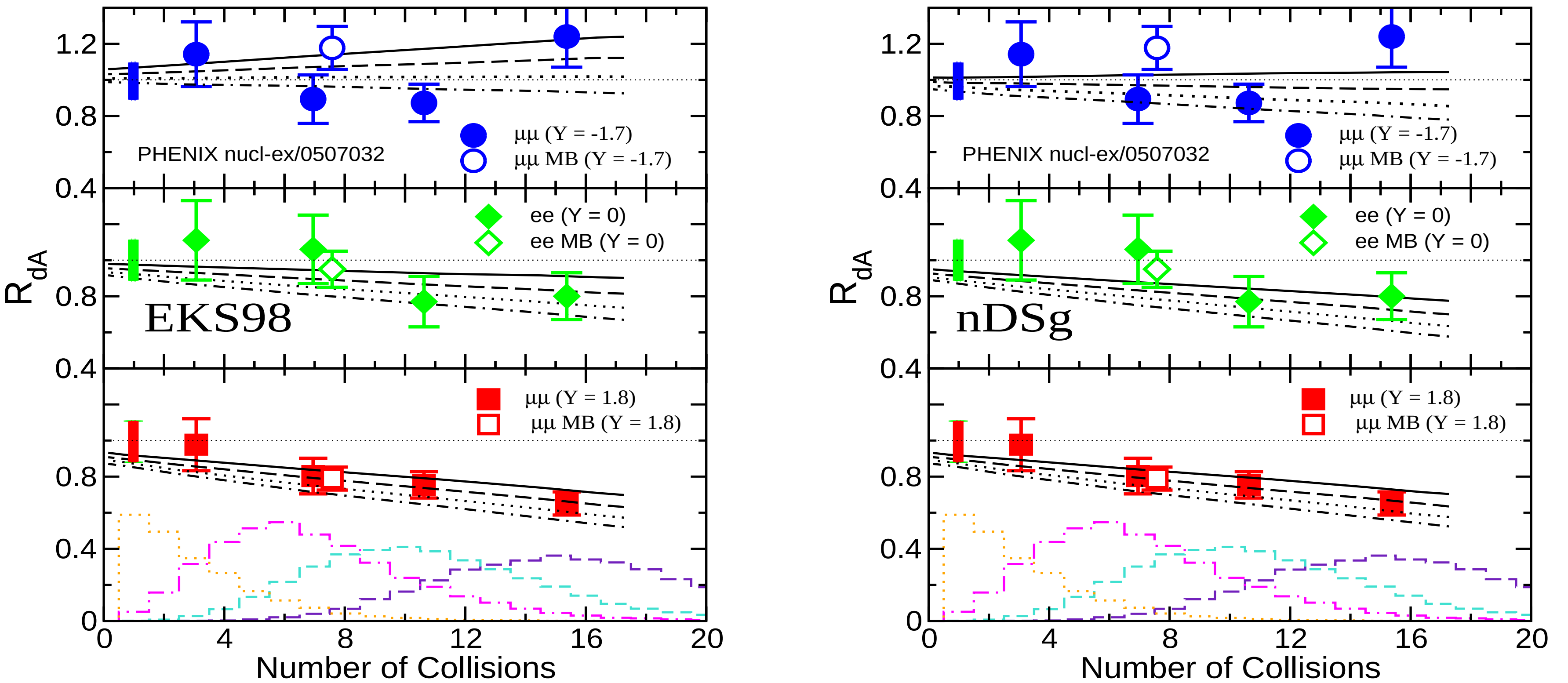

Figure 16: Octet absorption for $0 \leq \sigma_{\mathrm{abs}} \leq 3$ mb (upper to lower) calculated with EKS98 (left) and nDSg (right) with the MRST PDFs and $m = 1.2$ GeV, $\mu = 2m_T$. PHENIX data are shown for d+Au collisions at 200 GeV for $y = -1.7$ (top), 0 (middle) and 1.7 (bottom). (An additional 12% overall normalization error is not shown.) RV and Mike Leitch, in progress.

Absorption and Shadowing at RHIC: $R_{\mathrm{AA}}(N_{\mathrm{part}})$

Cold matter effects with $\sigma_{\mathrm{abs}} \sim 2-3$ mb in relatively good agreement with all but most central data

Room left for some dense matter effects

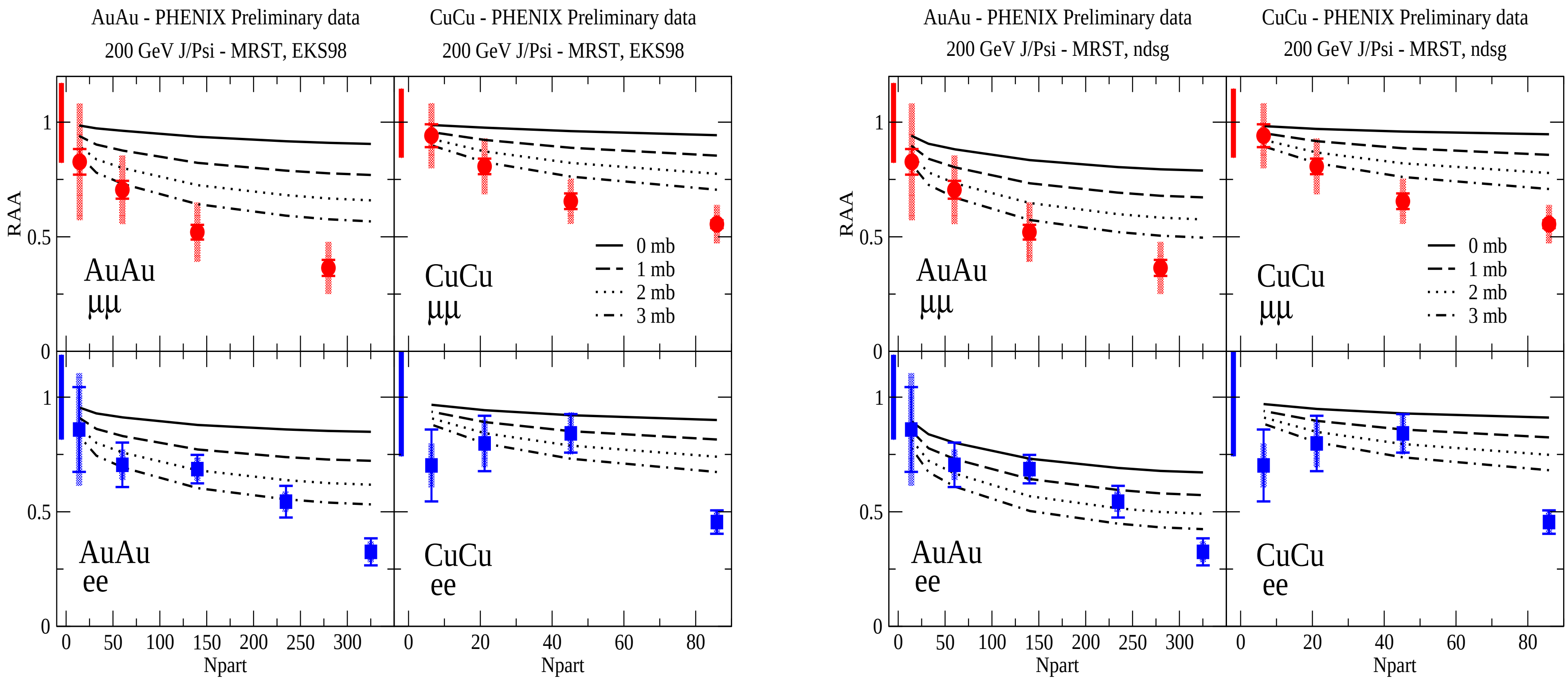

Figure 17: Octet absorption for $0 \leq \sigma_{\mathrm{abs}} \leq 3$ mb (top to bottom) calculated with EKS98 (left) and nDSg (right) with the MRST PDFs and $m = 1.2$ GeV, $\mu = 2m_T$. PHENIX data are shown for Au+Au and Cu+Cu collisions at 200 GeV in the forward $\mu\mu$ (upper) and central ee detectors. RV and Mike Leitch, in progress.

J/ψ Absorption and Shadowing in pPb at 8.8 TeV

Left: Effect of $\sigma_{\rm abs}$ for EKS98

Right: Comparing shadowing parameterizations for $\sigma_{\rm abs} = 2$ mb

Absorption small relative to shadowing

No rapidity shift included on pPb, assume pPb, pp at same $\sqrt{S}$

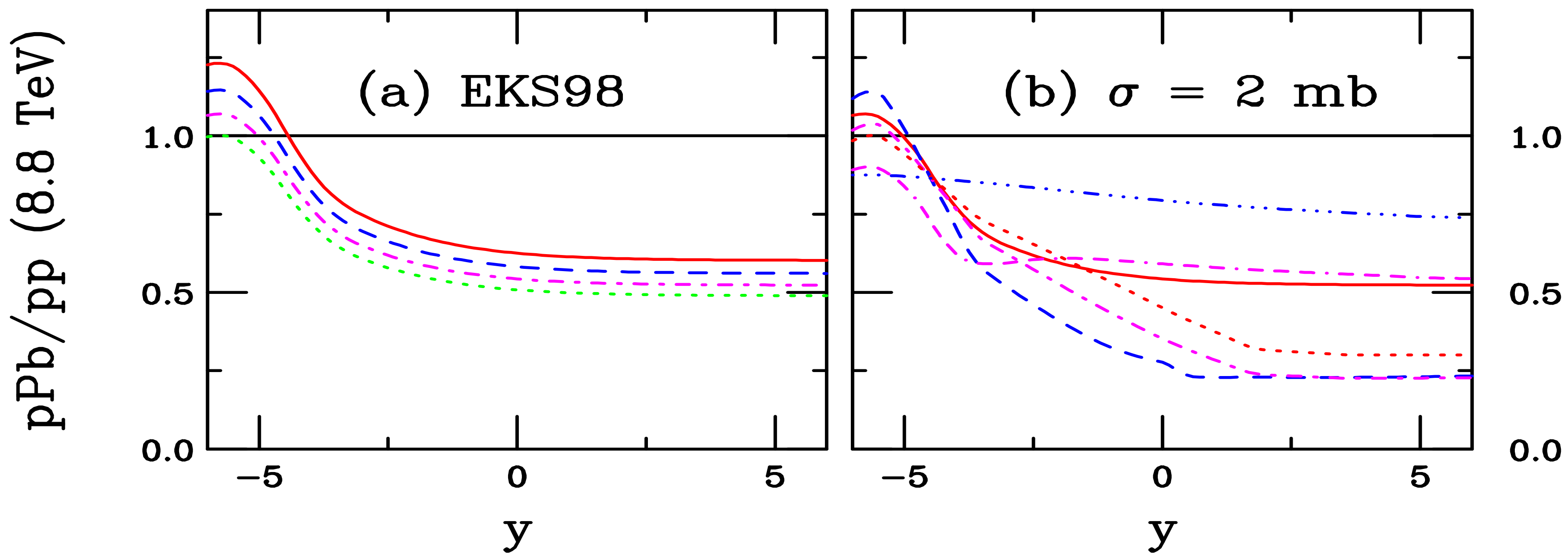

Figure 18: Left-hand side: The J/ψ pPb$/pp$ ratio at 8.8 TeV with the EKS98 shadowing parameterization for $\sigma_{\rm abs} = 0$ (solid red), 1 (dashed blue), 2 (dot-dashed magneta) and 3 (dotted green) mb. Right-hand side: Comparison of shadowing results for a 2 mb octet cross section with EKS98 (solid red), FGSo (dashed blue), FGSh (dot-dashed magenta), FGSl (dotted red), nDS (dot-dot-dot-dashed blue) and nDSg (dash-dash-dash-dotted magenta).

J/ψ Absorption and Shadowing in Pb+Pb at 5.5 TeV

Left: Effect of $\sigma_{\rm abs}$ for EKS98

Right: Comparing shadowing parameterizations for $\sigma_{\rm abs} = 2$ mb

Two nuclei produces two antishadowing peaks with dip in between

Assume Pb+Pb and pp at same $\sqrt{S}$

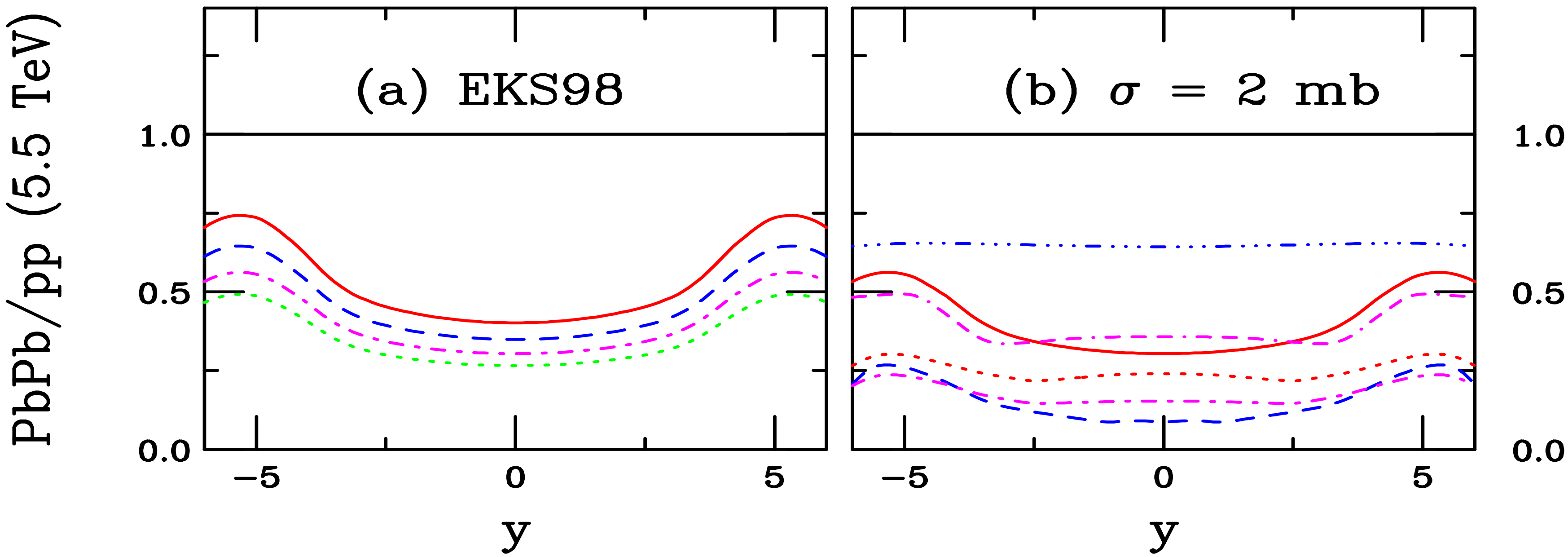

Figure 19: Left-hand side: The J/ψ Pb+Pb/pp ratio at 5.5 TeV with the EKS98 shadowing parameterization for $\sigma_{\rm abs} = 0$ (solid red), 1 (dashed blue), 2 (dot-dashed magneta) and 3 (dotted green) mb. Right-hand side: Comparison of shadowing results for a 2 mb octet cross section with EKS98 (solid red), FGSo (dashed blue), FGSh (dot-dashed magenta), FGSl (dotted red), nDS (dot-dot-dot-dashed blue) and nDSg (dash-dash-dash-dotted magenta).

Υ Absorption and Shadowing in pPb at 8.8 TeV

Left: Effect of $\sigma_{\rm abs}$ for EKS98

Right: Different shadowing for $\sigma_{\rm abs} = 1$ mb (lower because Υ smaller)

Antishadowing at larger y for Υ

Assume pPb and pp at same $\sqrt{S}$, no y shift

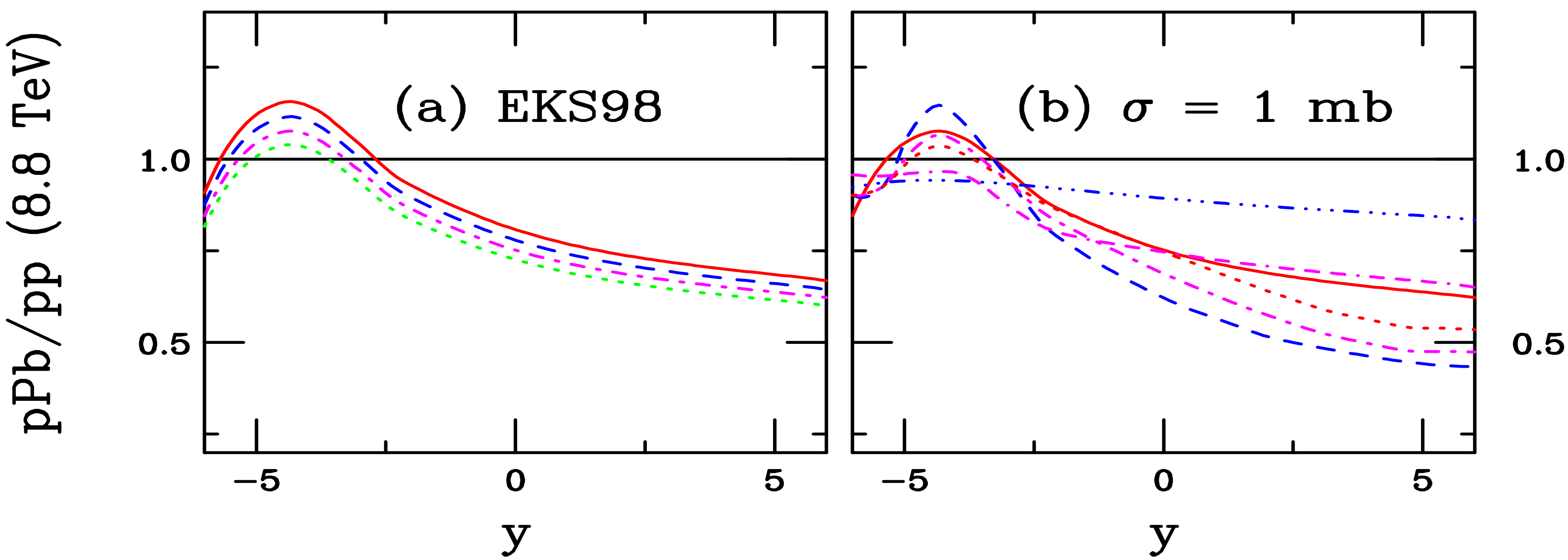

Figure 20: Left-hand side: The Υ pPb/pp ratio at 8.8 TeV with the EKS98 shadowing parameterization for $\sigma_{\rm abs} = 0$ (solid red), 0.5 (dashed blue), 1 (dot-dashed magneta) and 1.5 (dotted green) mb. Right-hand side: Comparison of shadowing results for a 1 mb octet cross section with EKS98 (solid red), FGSo (dashed blue), FGSh (dot-dashed magenta), FGSl (dotted red), nDS (dot-dot-dot-dashed blue) and nDSg (dash-dash-dash-dotted magenta).

Υ Absorption and Shadowing in Pb+Pb at 5.5 TeV

Left: Effect of $\sigma_{\rm abs}$ for EKS98

Right: Comparing shadowing parameterizations for $\sigma_{\rm abs} = 1$ mb

Antishadowing peaks closer than for J/ψ

Assume Pb+Pb and pp at same $\sqrt{S}$

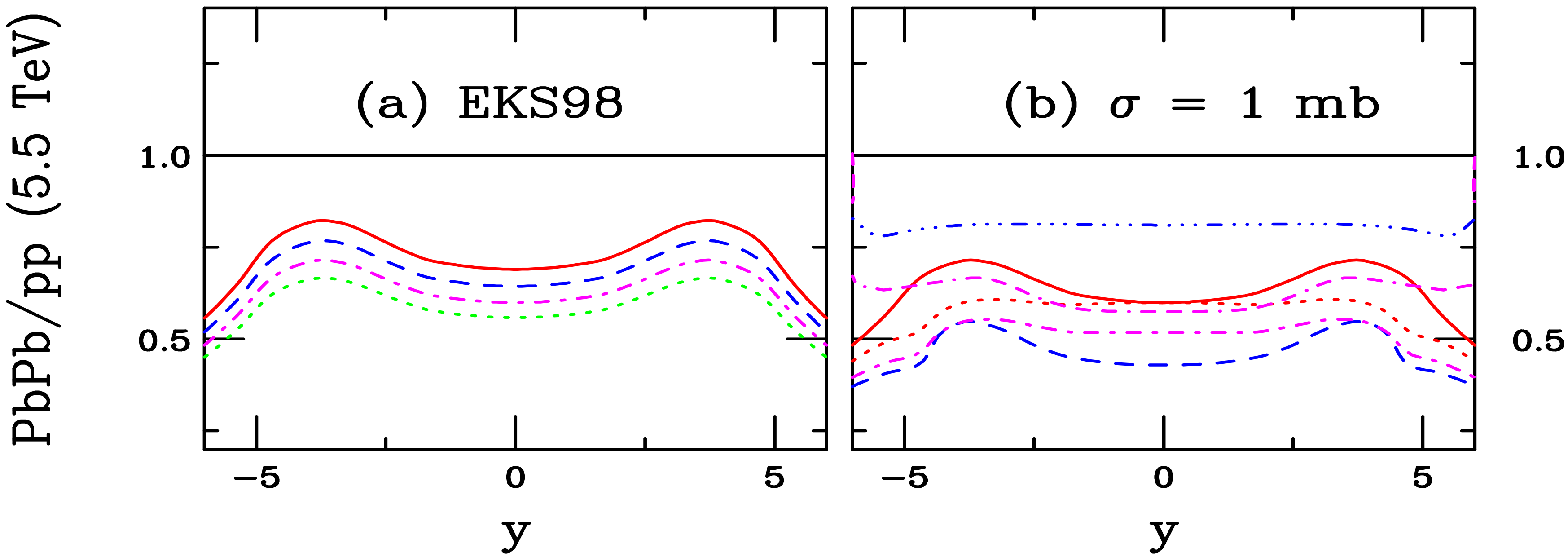

Figure 21: Left-hand side: The Υ Pb+Pb/pp ratio at 5.5 TeV with the EKS98 shadowing parameterization for $\sigma_{\rm abs} = 0$ (solid red), 0.5 (dashed blue), 1 (dot-dashed magneta) and 1.5 (dotted green) mb. Right-hand side: Comparison of shadowing results for a 1 mb octet cross section with EKS98 (solid red), FGSo (dashed blue), FGSh (dot-dashed magenta), FGSl (dotted red), nDS (dot-dot-dot-dashed blue) and nDSg (dash-dash-dash-dotted magenta).

Summary

- CEM useful tool for studying cold nuclear matter effects at RHIC
- Measurement of χ_c A dependence would provide clear test of absorption mechanism
- Current d+Au J/ψ data agree well with combination of initial state shadowing and final state absorption
- Need better statistics to distinguish between shadowing parameterizations and determine strength of absorption
- Cold matter effects need to be accounted for in AA collisions but room for dense matter effects
- Υ measurements at LHC should further probe x and Q^2 dependence of initial state effects with less absorption
- LHC pA program needed to fix level of cold matter effects on the TeV scale